Journal of Crystal Growth ▮ (▮▮▮▮) ▮▮▮–▮▮▮

Contents lists available at ScienceDirect

Journal of Crystal Growth

journal homepage: www.elsevier.com/locate/jcrysgro

Single-crystal growth of $LiMnPO_4$ by the floating-zone method

Nadja Wizent [a,*], Günter Behr [a], Ferdinand Lipps [a], Ingo Hellmann [a], Rüdiger Klingeler [a], Vladislav Kataev [a], Wolfgang Löser [a], Norio Sato [b], Bernd Büchner [a]

[a] IFW Dresden, Leibniz Institute for Solid State and Materials Research, D-01171 Dresden, Germany
[b] Toyota Motor Europe, Technical Centre, Hoge Wei 33, B-1930 Zaventem, Belgium

ARTICLE INFO

Article history:
Received 5 August 2008
Received in revised form
7 January 2009
Accepted 13 January 2009
Communicated by V. Fratello

PACS:
81.10.Fq
75.50.Ee
75.30.Gw
76.30.−v

Keywords:
A1. Morphological stability
A2. Floating-zone technique
B1. Lithium compounds
B1. Phosphates

ABSTRACT

$LiMnPO_4$ crystals with orthorhombic Pnma crystal structure containing large grains have been grown successfully for the first time by the traveling-solvent floating-zone technique under elevated argon pressure. The grains achieve sizes of about $3\,mm^2 \times 10\,mm$ and display an orange transparent color. During the growth process, the traveling zone is continuously enriched with PO_4- and Li-ions, due to the self-adjustment of the liquid zone, which hinders grain selection and leads to constitutional supercooling with the formation of a secondary phase in a later stage of the process. Magnetic measurements performed on oriented cuboids reveal antiferromagnetic ordering of the Mn^{2+}-ions below $T_N \approx 34\,K$. The *c*-axis is the easy magnetic axis.

1. Introduction

The opportunity of carbon dioxide free energy supply for motor vehicles is a new field of research [1] because of the limitation of oil upstream, climate warming and CO_2 emission. Presently, rechargeable lithium batteries are the most efficient energy storage system known and the next generation of low-cost materials with higher charge–discharge rates is being explored. Research in lithium transition metal phosphates $LiMPO_4$ (M=Co, Fe, Mn and Ni) is promising, especially for $LiFePO_4$ materials [2]. Apart from the electrochemical properties, which are the key issues for use as active materials for Li-ion batteries, other important factor is the magnetism in these compounds [3–5]. Magnetic properties are determined by the electronic states and may thus reflect the potential differences within the $LiMPO_4$ family. Some magnetic properties of $LiMPO_4$ were already studied in the early 1960s. So far, most investigations have been performed on polycrystals, e.g., in $LiFePO_4$ and $LiMnPO_4$ powder samples prepared by a sol–gel method [6]. The crystal structure of the compounds $LiFePO_4$ and $LiMnPO_4$ is orthorhombic with the space group Pnma (Fig. 1) [7]. $LiFePO_4$ single crystals were grown by the FZ method under an argon flow by Chen et al [8]. A faster growth velocity was applied because volatilization of Li may cause a non-stoichiometry or decomposition of the compound. Moreover, evaporation of Li was reported for sintering above 500 °C. The melting range of $LiFePO_4$ between 887 and 942 °C is quite low. According to our differential thermoanalysis measurements $LiMnPO_4$ melts at 1019 °C. Therefore, we expect an increased tendency of vaporization. In $LiFePO_4$ the antiferromagnetic transition [9,10] occurs at 52 K with magnetic moments aligned along the [0 1 0] crystal axis. $LiMnPO_4$ was suggested to be a collinear antiferromagnet with a Néel temperature ranging between 35 K, for synthetic materials [4], and 42 K, for minerals [11]. Although single-crystal growth of $LiMnPO_4$ by a flux method [12] was already accomplished in 1969, no appropriate measurements of anisotropic magnetic properties are reported so far, probably because of the small size of the crystals grown. Only recently, bulk $LiCoPO_4$ single crystals (5 mm in diameter) were grown by an optical floating-zone technique [13].

Here, we will consider single-crystal growth of the $LiMnPO_4$ compound prepared by an optical floating-zone method. Oriented single-crystalline samples have been utilized for studying the antiferromagnetic behavior of $LiMnPO_4$.

*Corresponding author. Tel.: +49 351 4659 562; fax: +49 351 4659 313.
E-mail address: n.wizent@ifw-dresden.de (N. Wizent).

0022-0248/$ - see front matter © 2009 Elsevier B.V. All rights reserved.
doi:10.1016/j.jcrysgro.2009.01.090

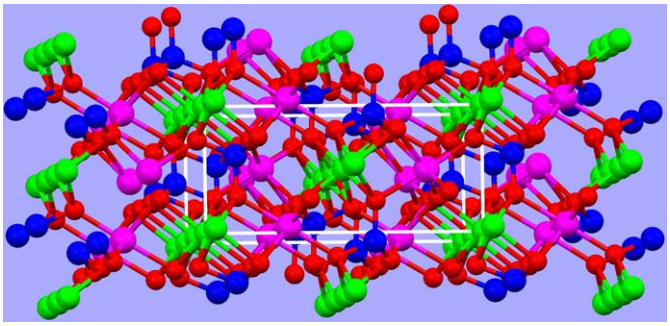

Fig. 1. Crystal structure (Pnma) of $LiMnPO_4$.

2. Experimental Procedure

Different powder preparation routes have been examined to obtain a single phase compound material. Intermediate X-ray analyses have been conducted to verify the powder quality. Using Li_2CO_3 (Chempur 99+%), $MnCO_3$ (Alfa Aesar 99.9%) and $NH_4H_2PO_4$ (Chempur 99+%) as starting materials it was not possible to get single phase compound powder. In this case, single-crystal growth by traveling-solvent floating-zone (TSFZ) technique failed. Synthetic powder has been finally obtained by mixing and grinding Li_3PO_4 (Chempur 99+%), $MnCO_3$ (Aldrich 99.9+%) and $NH_4H_2PO_4$ (Chempur 99+%) in nominal molar ratios corresponding to stoichiometric $LiMnPO_4$. The powder was sintered several times at 800 °C for 48 h in Ar atmosphere with intermediate grinding. The single phase powder exhibits an orange-white color. It has been pressed into polycrystalline rods (EPSI Engineered Pressure Systems; 3500 bar) in latex tubes with a diameter of 6 mm and sintered again at 800 °C for 34 h.

The floating-zone crystal growth was accomplished in a vertical optical furnace URN-2ZM (MPEI, Moscow) [14] and alternatively in the new Smart Floating Zone (SFZ) facility designed and constructed at IFW Dresden [15]. In both methods, a 5 kW xenon lamp is utilized for heating the zone. The construction of the growth chambers made from quartz enable the use of high-pressure gas atmospheres. In the present case, 40 bars Ar pressure avoids Li_2O vaporization and the oxidation of Mn^{2+} to Mn^{3+}. Counter-rotation of feed rod (15 rpm) and crystal (25 rpm) has been applied, which improves mixing of the melt in the floating zone.

During the growth process, the temperature of the floating zone has been measured with a two-color pyrometer by using a novel stroboscopic method [16]. For stable growth, the temperature of the circumference of floating zone was held between 1100 and 1150 °C. The operating temperature is considerably higher than for crystal growth of $LiFePO_4$ and requires elevated Ar gas pressure to prevent vaporization of LiO_2. Axial temperature gradients on the lower rod (G_{lr}~85±10 K/mm) and upper rod (G_{ur}~90±10 K/mm) were determined by moving the pyrometer vertically along the rod axis. The high-temperature gradients could be one reason for the crack formation that occurs shortly after solidification. This might be solved by applying an after heat treatment during the growth process.

A number of floating-zone experiments with different growth rates ranging from 1 to 10 mm/h have been conducted in order to improve the perfection of the grown crystals, especially to avoid (or to reduce) crack formation during cooling. Microstructure and crystal perfection were examined by optical metallography in polarized light and scanning electron microscopy (SEM). The X-ray Laue back-scattering method was utilized to determine the crystal orientation. Some crystals were annealed at 680 °C for 72 h to reduce the Li-content, and therefore to increase the electrical conductivity.

Oriented cuboid specimens for magnetic measurements were cut from the crystals prepared. Magnetic susceptibility $\chi(T)$ measurements in the presence of a magnetic field (H) of 100 Oe were carried out in the temperature interval 2–350 K with a Quantum Design MPMS SQUID magnetometer. Electron spin resonance (ESR) measurements on a single crystal of $LiMnPO_4$ have been performed with a commercial Bruker Spectrometer EMX-Series at a frequency of 9.5 GHz and magnetic fields 0–10 kOe in the temperature range 4–300 K.

3. Crystal growth and perfection

In Fig. 2, the image of a $LiMnPO_4$ crystal grown with 10 mm/h is shown. Because of the transparency of the crystal and also because of its illumination through the liquid zone by the vertical light flux from above, a concave interface between crystal and liquid zone is formed. It can be observed during the growth process and it is also proved by a longitudinal section through the rod. The quenched liquid zone is visible on the left-hand side of Fig. 2a. The concave interface shape disables a proper grain selection, which leads to big columnar grains of 3–4 mm × 2 mm in cross-section and some cm in length a few mm after the start of the growth process. The facets on the rod surface point to the single-crystalline nature of large parts of the grown rod (cf. Fig. 2a). The optical micrograph Fig. 2b reveals that the as-grown rod is not single crystalline throughout the entire cross-section, but it consists of a few large grains. The largest grain on the left-hand side covers nearly one half of the cross-section, but it is cracked into two parts. The grains on the right-hand side were broken out of the rod section during the metallographic preparation process. Therefore, only the embedding resin (with dark bubbles inside) is visible. The X-ray Laue back scattering images of large individual grains (Fig. 3) provide reflections, which correspond to the simulated pattern of the orthorhombic Pnma space group (Fig. 1) and prove the single-crystalline nature of the individual grains. The crystallographic structure was further investigated by a four circle diffractometer. The lattice parameters of the orthorhombic space group Pnma (at T=150 K) are given and compared with available literature data in Table 1. The lattice parameters agree fairly well with polycrystals. The slightly smaller values of crystals

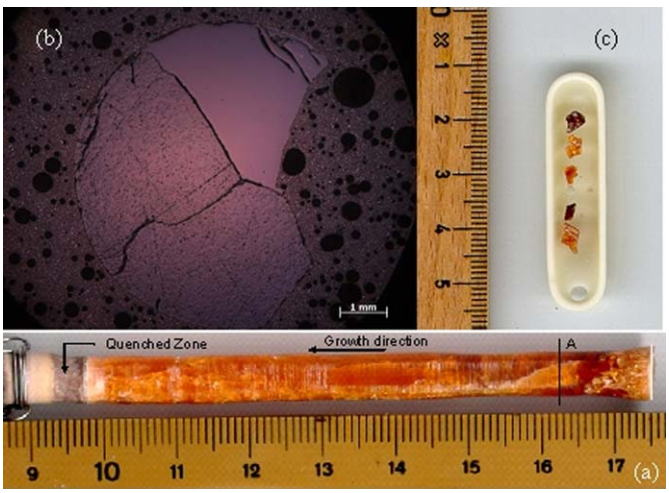

Fig. 2. (a) $LiMnPO_4$ crystal grown with 10 mm/h. The growth direction and the quenched last zone are indicated. (b) Cross-sectional optical image in polarized light at A (the surrounding parts with dark bubbles represent the embedding resin). (c) Single-crystalline large grains after annealing 72 h at T=680 °C.

Please cite this article as: N. Wizent, et al., J. Crystal Growth (2009), doi:10.1016/j.jcrysgro.2009.01.090

are probably due to a different reference temperature of polycrystals, which were studied at room temperature [6].

The comparison of X-ray Laue back scattering images of the two grains shown in Fig. 2b elucidated their sizeable orientation differences of 2°, 37° and 59° with respect to the three main axes of the orthorhombic system [1 0 0], [0 1 0] and [0 0 1], respectively. Unfortunately, growth proceeds the parasitic grains do not grow out, and therefore no single crystal throughout the cross-section was formed. One possible reason is grain boundary segregation. Near the end of the growth process a second phase was detected at the grain boundaries, which eventually stabilizes the grains [17]. Towards the end of the growth process the second phase formation in the $LiMnPO_4$ matrix (dark inclusions in Fig. 4) can even deteriorate the growth of big grains. The amount of the minority phase is too small to be analyzed by powder diffraction or chemical analysis methods. However, WDX analyses (without normalization to 100%) provide a rough idea of its composition and hint to a Mn-depleted phase.

Due to the asymmetry of the light flux in our growth configuration, the crystallization process depends on the growth direction [14]. Light coming from the top of the upper mirror shines through the transparent liquid leading to a concave phase boundary for downward growth of the crystal. For a crystal grown up side down the incident light does not affect the phase boundary. In this case, a convex phase boundary was observed. Constitutional supercooling and cellular growth can arise at the growth interface because of the composition difference between crystal and floating zone (Fig. 4). The chemical analysis of the crystal is difficult, because Li is a light element and, therefore, its content cannot be accurately determined by microprobe analysis, neither in the EDX nor in the WDX mode. Chemical analyses (ICP-OES) of a bulk specimen show a deficit of Li and PO_4 in the crystal balanced by excess Mn. On the other hand, in the quenched liquid zone a complementary deficit of Mn and an enrichment of Li and PO_4 were detected. During the growth the melt is continuously enriched with PO_4-ions. If a critical concentration difference is exceeded, constitutional supercooling arises. This may explain why the grain selection gets worse at the end of the growth process.

Although we did not succeed in the preparation of perfect single-crystalline rods, the coarse grains turned out to be large enough for cutting large single-crystalline cuboids of several mm^3 in size, which were oriented and utilized for various magnetic measurements. Some large single crystals, shown in Fig. 2c were also subjected to an annealing treatment of 72 h at T=680 °C. The magnetic properties of annealed specimen were compared with as-grown samples. Although the color of the crystal has been changed during annealing from orange to dark purple, no magnetic effect could be discovered in the specimens as shown below.

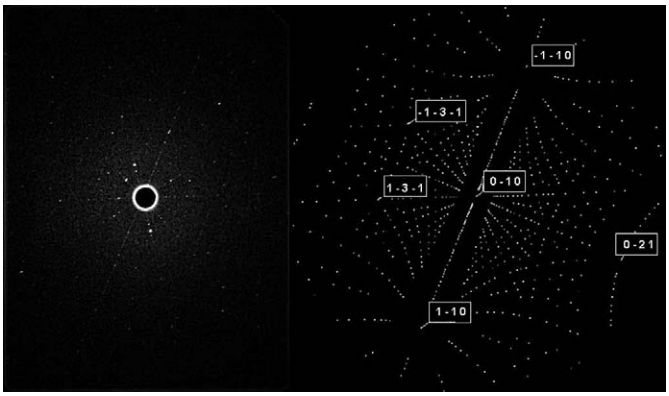

Fig. 3. X-ray Laue back scattering image of a large grain on the cross-section of a $LiMnPO_4$ crystal with main reflections. Left: Laue pattern; Right: simulation of the Laue pattern.

Table 1
Lattice parameters.

	a (Å)	b (Å)	c (Å)	T (K)
Geller and Durand [3] polycrystal	10.46	6.10	4.774	–
Arcon et al. [6] polycrystal	10.447(6)	6.11018(3)	4.7431(3)	Room temperature
Present results, single crystal	10.419(1)	6.0881(7)	4.7304(5)	150 K

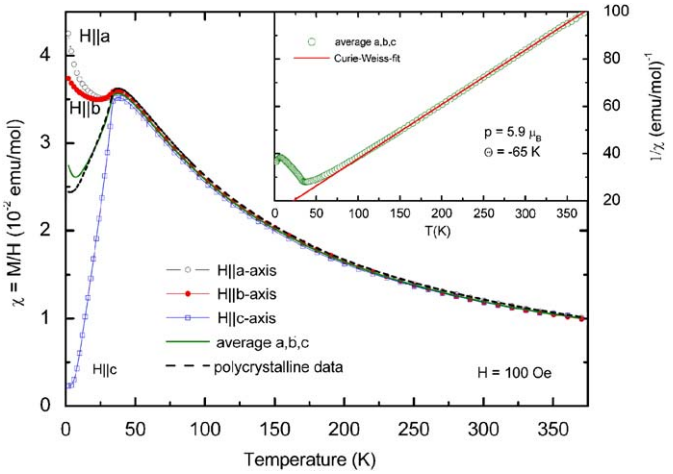

Fig. 5. Temperature dependence of the static susceptibility $\chi(T)$ with the external magnetic field of H=100 Oe oriented along the three crystal axes, i.e. $H\|a$, $H\|b$ and $H\|c$, respectively. In addition, the averaged susceptibility of the crystal is compared with a polycrystalline sample. Inset: Inverse averaged susceptibility and a Curie–Weiss fit to the data (see the text).

Fig. 4. Vertical section through the end of crystal (bottom) showing: (a) a concave crystal–melt interface for downward growth, (b) a convex interface for upward growth and (c) scale up of (b) showing cellular growth of the crystal-melt interface ahead the molten zone (top).

Please cite this article as: N. Wizent, et al., J. Crystal Growth (2009), doi:10.1016/j.jcrysgro.2009.01.090

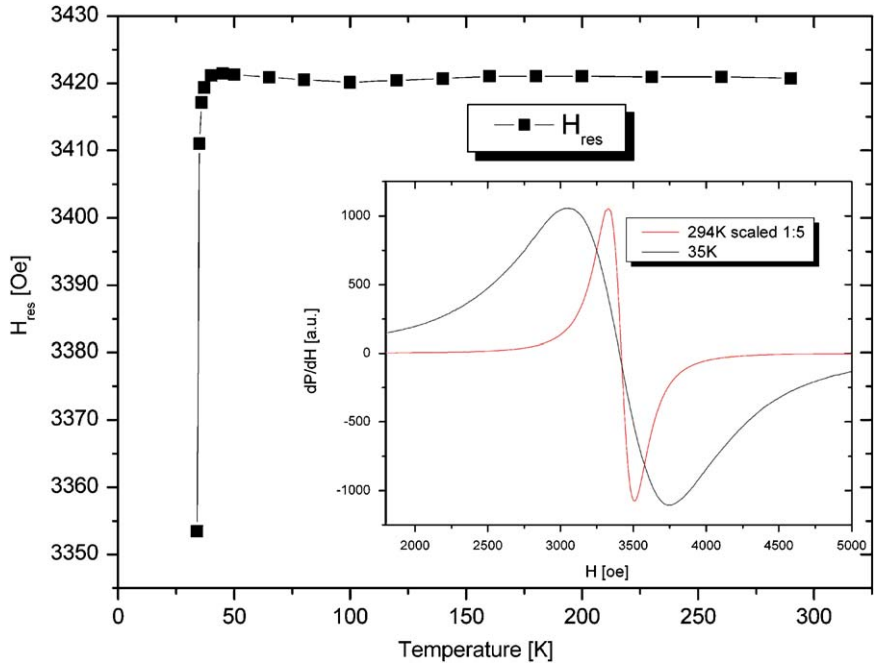

Fig. 6. Inset: Representative ESR signals (field derivative of the absorbed microwave power $dP(H)/dH$) at 35 and 294 K. Main panel: Temperature dependence of the resonance field H_{res}.

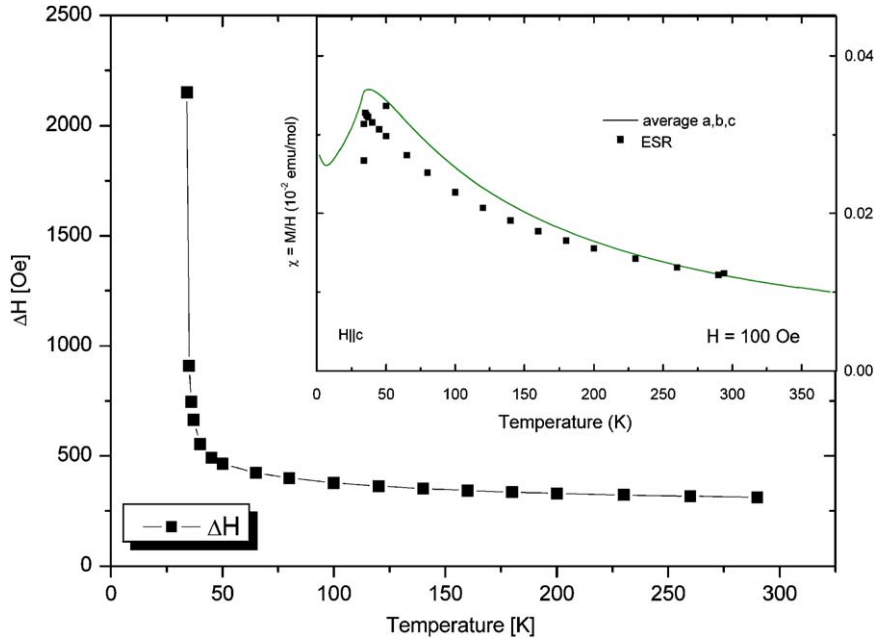

Fig. 7. Main panel: temperature dependence of the ESR linewidth ΔH. Inset: Temperature dependence of the static susceptibility $\chi(T)$ plotted together with the ESR intensity I_{ESR} (black squares). The averaged susceptibility of the crystal is compared with ESR data.

4. Magnetic properties

The magnetic properties of single-crystalline $LiMnPO_4$ samples were characterized by static magnetization measurements as well as ESR spectroscopy. In Fig. 5, the temperature dependence of the magnetic susceptibility $\chi=M/H$ is shown for the three crystal orientations, $H \parallel \langle 100 \rangle$ (a-axis), $H \parallel \langle 010 \rangle$ (b-axis) and $H \parallel \langle 001 \rangle$ (c-axis). In addition, the average of the susceptibility measured along the three crystal axes is displayed. Note that the calculated average of single-crystal data coincides with experimental susceptibility data of a powder sample in the whole temperature regime. The data demonstrate a Curie–Weiss behavior at high temperatures, which is illustrated by the inverse susceptibility data shown in the inset of Fig. 5. Fitting the data in terms of a Curie–Weiss law

$$\chi = \frac{C}{T - \Theta}$$

yields an effective moment $p=5.9\,\mu_B$ and a Curie–Weiss temperature $\Theta=-65$ K. The observed value of p implies a spin $S=\frac{5}{2}$ if the g-factor of 1.98 (see below) is considered.

Please cite this article as: N. Wizent, et al., J. Crystal Growth (2009), doi:10.1016/j.jcrysgro.2009.01.090

The magnetization data, therefore, clearly confirm the mean valence 2+ of the Mn-ions.

Upon cooling below ~120 K the magnetization starts to deviate from the Curie–Weiss behavior (cf. inset of Fig. 5), which is consistent with the observation of an antiferromagnetic Curie–Weiss temperature. Eventually, long range antiferromagnetic spin order is found below $T_N \approx 34$ K. The measurements on single-crystalline specimens elucidate the nearly uniaxial magnetic anisotropy of $LiMnPO_4$. The magnetic easy axis is along the *c*-axis where the magnetic susceptibility displays a sharp drop-off upon cooling below 34 K.

For electron spin resonance measurements the direction of the magnetic field was set perpendicular to the [0 1 0] of the crystalline $LiMnPO_4$ sample. The ESR spectrum consists of a single line of a Lorentzian shape (inset to Fig. 6). From the fit of the line profile the field of resonance H_{res} (Fig. 6), width ΔH and intensity I_{ESR} of the signal (Fig. 7) have been determined.

The ESR intensity is proportional to the magnetic susceptibility of the resonating spins. Therefore, I_{ESR} for $LiMnPO_4$ follows closely the temperature dependence of the susceptibility obtained from measurements of the static magnetization (Fig. 7). This gives evidence that ESR probes the same spins which determine the static magnetic properties of $LiMnPO_4$. In the broad temperature range 40–300 K, H_{res} is practically constant and amounts to $H_{res} \sim 3420$ Oe (Fig. 6). This corresponds to an effective *g*-factor of 1.98 which is very typical for Mn^{2+} ions. The width of the signal in the same temperature range increases from $\Delta H \sim 300$ Oe at 300 K to $\Delta H \sim 600$ Oe at 40 K (Fig. 7). However, a further decrease of temperature yields a much stronger broadening of the signal accompanied with a significant shift of H_{res} to low field values (Figs. 6 and 7). The signal is not observable below 34 K.

Such a behavior of ESR parameters in the low-temperature regime is very typical for a concentrated paramagnet, which approaches a phase transition to a three-dimensional antiferromagnetically ordered state. The occurrence of this phase transition at 34 K is documented by static magnetic measurements (Fig. 5, inset to Fig. 6). The disappearance of the ESR signal at the phase transition is due to the opening of the antiferromagnetic energy gap for resonance excitations, which is larger than the ESR frequency of 9.5 GHz used in the present work.

In the paramagnetic regime above 34 K the Lorentzian shape of the signal and its relatively small width give evidence for a strong isotropic exchange interaction between the spins of manganese. This together with the occurrence of the critical behavior close to the magnetic ordering temperature strongly suggests that ESR in $LiMnPO_4$ is dominated by magnetic interactions within the manganese spin system and is not sensitive to the dynamics of Li-ions. ESR spectroscopy is hence not informative regarding characterization of the Li subsystem.

As mentioned above several crystals have been annealed for 72 h at 630 °C. Two of them have changed their color (Fig. 2c) and suggest some change in their electronic structure. However, there was virtually no change in magnetic properties compared with as-grown crystals. This indicates that electronic changes responsible for the different color might occur at the crystal surface while the bulk material which dominates the magnetic properties of the crystal is hardly affected by annealing.

5. Conclusions

Single crystals of $LiMnPO_4$ several mm^3 in size have been grown by the traveling-solvent floating-zone technique under high Ar pressure. The grain selection is disabled by a Mn-depleted secondary phase to the end of the growth process. However, good-quality crystals could be analyzed by powder diffraction, four circle diffractometer and physical measurements. Magnetic measurements on oriented samples proved the magnetic easy axis along the *c*-axis and an antiferromagnetic ordering with $T_N \approx 34$ K comparable to previous NMR measurements [18]. Annealing of crystals lead to a change in color but leave the magnetic behavior virtually unaffected. However, it has no consequence on magnetic data, so we think that it is only a surface effect.

Acknowledgements

The authors thank M. Deutschmann, S. Pichl, S. Mueller-Litvanyi and S. Gaß for experimental assistance and A. Voß for chemical analyses.

References

[1] K.T. Fehr, Phys. Chem. Minerals. 34 (2007) 485.
[2] S.Y. Chung, Nature Materials. Mater. 1 (2002) 123.
[3] S. Geller, J.L. Durand, Acta Cryst. 13 (1960) 325.
[4] R.M. Bozorth, V. Kramer, International colloquium of magnetism in. Colloq. Magn. Grenoble (1959) 329.
[5] F. Zambonini, L. Malossi, Z. Krist, 80 (1931) 442.
[6] D. Arcon, A. Zorko, R. Dominko, Z. Jaglicic, J. Phys. Condens. Matter 16 (2004) 5531.
[7] S. Geller, J.L. Durand, Acta Cryst. 13 (1960) 325.
[8] D.P. Chen, A. Maljuk, C.T. Lin, J. Cryst. Growth 284 (2005) 86.
[9] W.L. Bond, Rev. Sci. Instrum. 25 (1954) 401.
[10] C. Kittel, Introduction to Solid-State Physics, 2nd ed, Wiley Inc, New York, 1956 p. 571.
[11] E.R. Andrew, Nuclear Magnetic Resonance, Cambridge University Press, Cambridge, England, 1955, pp. 185–190.
[12] P.R. Elliston, J. Phys. Chem. Solids 30 (1969) 1335.
[13] R. Saint-Martin, S. Franger, J. Cryst. Growth 310 (2008) 861.
[14] D. Souptel, W. Löser, G. Behr, J. Cryst. Growth 300 (2007) 538.
[15] G. Behr, W. Löser, D. Souptel, et al., J. Cryst. Growth 310 (2008) 2268.
[16] G. Behr, et al., German Patent DE 10 2006 019 807.7 (21.04.2006) and PCT/EP2007/05157 (07.03.2007).
[17] I. Mazilu, M. Frontzek, W. Löser, G. Behr, A. Teresiak, L. Schultz, J. Cryst. Growth 275 (2005) e103.
[18] J.M. Mays, Phys. Rev. 131 (1963) 38.

Please cite this article as: N. Wizent, et al., J. Crystal Growth (2009), doi:10.1016/j.jcrysgro.2009.01.090